SIMULATION OF THE ATTITUDE BEHAVIOUR AND AVAILABLE POWER PROFILE OF THE DELFI-C^3 SPACECRAFT WITH APPLICATION OF THE OPSIM PLATFORM

F. te Hennepe, B.T.C. Zandbergen, R.J. Hamann
Chair of Space Systems Engineering, Faculty of Aerospace Engineering, Delft University of Technology
Kluyverweg 1, 2629 HS, Delft
The Netherlands
f.tehennepe@delfic3.nl, b.t.c.zandbergen@tudelft.nl, r.j.hamann@tudelft.nl

ABSTRACT

Delfi-C^3 is a nanosatellite being developed by the Faculties of Aerospace Engineering and Electrical Engineering of Delft University of Technology. Its primary mission is to serve as a test platform for various technology payloads. Delfi-C^3 is scheduled for a piggyback launch into a near-circular sun-synchronous orbit in September 2007.

To simulate the attitude behaviour and the available electrical power of the spacecraft, use is made of OpSim. This is a simulation platform based on the EuroSim platform developed by Dutch Space. It allows for accurate simulation of spacecraft orbits by a powerful numerical integration subroutine and detailed physical modelling. Therefore, individual algorithms modelling the attitude dynamics and the generated power were added for determining the attitude behaviour and electrical power. This makes OpSim an even more powerful tool for general spacecraft simulation.

Delfi-C^3 uses passive attitude control by applying rods of magnetic material. Delfi-C^3 is subjected to various disturbance torques. By using the OpSim platform the magnitudes of the disturbance torques and the magnetic control torque have been determined.

In addition, OpSim is capable of determining the amount of solar and albedo power, which is incident to the solar arrays of the spacecraft. Therefore, the amount of power received by the spacecraft in its orbital path has been determined.

In this paper, the processes of modelling the disturbance torques acting on Delfi-C^3 and its available electrical power are presented. Furthermore, various results of the operational simulations in OpSim are shown. These results are compared to the design requirements of Delfi-C^3 with respect to minimum required power and maximum allowed acceleration rate. A conclusion is drawn whether Delfi-C^3 will be successful in performing its mission in these aspects.

KEYWORDS

Delfi-C^3, operational simulation, attitude control, disturbance torques, power evaluation

1 INTRODUCTION

Simulation is an important design tool in a spacecraft development process. It allows for preliminary evaluation of the spacecraft performance without the necessity of performing time and money consuming verification tests. An all-embracing simulation is the so-called operational simulation, in which the behaviour of the spacecraft is modelled as if it were in orbit around the Earth.

Operational simulations have been performed for the Delfi-C^3 nanosatellite. These are accomplished on the OpSim simulation platform, which is a powerful numerical integration tool used for modelling spacecraft orbits. It was originally developed for developed for Delfi-1, and later extended to Delfi-C^3 [1][2][3]. Quantities of interest are the attitude behaviour of the spacecraft and the generated array power. To model these quantities, dedicated subroutines had to be developed.

In this paper, the modelling of the various relevant parameters in the OpSim simulator is explained. In section 2 , the Delfi-C^3 spacecraft is shortly introduced. In section 3, the body fixed reference frame and the set of equations used for attitude dynamics are introduced. A description of the control torque is given in section 4, while the disturbance torques are treated in section 5. The algorithm used for evaluating available power is illustrated in section 6. Several simulation results are shown in section 7.

2 DELFI-C^3 SPACECRAFT

Delfi-C^3, see figure 1, is a nanosatellite developed by students of the Faculties of Aerospace Engineering and Electrical Engineering of Delft University of Technology under supervision of faculty staff. As such, it is an educational opportunity for students to obtain experience in a spacecraft development process [4].

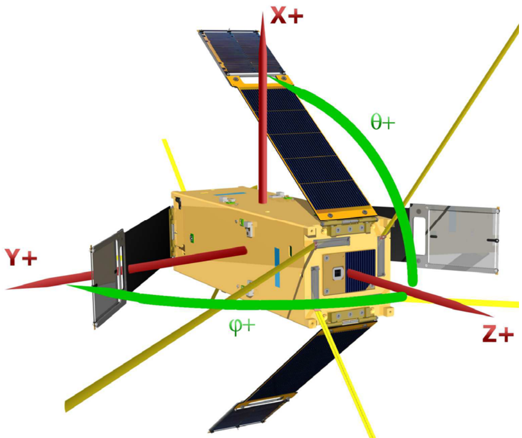

FIG 1: Delfi-C^3 spacecraft with body fixed reference frame

General characteristics of the satellite are given in the table 1.

TAB 1: General characteristics of the Delfi-C^3 spacecraft

Parameter	Characteristic/value
Length	326.5 mm
Width	100.0 mm
Height	100.0 mm
Mass	2.2 kg
Communication	Omnidirectional
Attitude	Coarse attitude control
Power consumption in sunlight	2.5 W
Power consumption in eclipse	0 W

Delfi-C^3's primary mission is to serve as a testbed platform for a number of innovative technologies:

- An innovative type of thin-film solar cells developed by Dutch Space;
- An autonomous wireless sun sensor developed by TNO Science & Industry;
- A Radio Amateur Platform transponder designed by the Faculty of Electrical Engineering of Delft University of Technology and the Technische Hogeschool Rijswijk.

For electrical power generation, Delfi-C[3] uses four solar arrays, which, as a minimum, should provide for 3 W of array power in sunlit conditions. Power conditioning is achieved by a custom designed shunt switching regulator [5].

Attitude control is passive by means of hysteresis rods and a single permanent magnet. The main purpose of the hysteresis rods is to enforce upper and lower boundaries on the rotational velocity following orbit insertion. Additionally, coarse attitude control is achieved, thereby allowing for all experiments to receive sunlight, although not necessarily at the same time and continuously [6].

Delfi-C[3] is scheduled for a piggyback launch into Low Earth Orbit with an Indian PSLV (Polar Satellite Launch Vehicle) launcher from Sriharikota in September 2007. Table 2 lists the characteristics of the Delfi-C[3] orbit.

TAB 2: Orbit characteristics of the Delfi-C[3] spacecraft

Parameter	Value
Orbital altitude	635 km
Inclination	97.91 °
Eccentricity	~0
Local time ascending node	10.30 AM

3 ATTITUDE DYNAMICS

3.1 Reference frame

For the simulations, use is made of the so-called body fixed reference frame. This coordinate system is shown in figure 1.

The *z*-axis of the body fixed reference frame runs parallel to the satellite's long dimension. The *x*-axis is perpendicular to the *z*-axis. Its positive direction is going in such a way that the quadrant constituted by the positive *z*- and *x*-axes contains a solar panel hinge. The *y*-axis completes the right handed orthogonal coordinate system. Its origin is situated at the geometrical center of the spacecraft.

3.2 Dynamics and kinematics

Attitude dynamics of the Delfi-C[3] spacecraft are modelled in the OpSim simulator by a complete set of kinematic and dynamic equations [7]. By using these equations, the influence of the torques on the attitude behaviour of the spacecraft is implemented.

For calculating the rotational acceleration of the spacecraft, the following expression is applied.

(1) $$\vec{M} = \hat{J}\dot{\vec{\omega}} + \vec{\omega} \times \hat{J}\vec{\omega}$$

where $\vec{M}$ is the sum of the control and the disturbance torque vector, $\hat{J}$ is the spacecraft's inertia tensor, and $\vec{\omega}$ is the rotational rate of the spacecraft.

This expression relates the torques acting on the spacecraft to a rotation in the body fixed reference frame. These rotations are transformed to time derivatives of the Euler angles by using the following transformation expression:

(2) $$\vec{\omega} = C\dot{\vec{\theta}}$$

where $\dot{\vec{\theta}}$ is the time derivative vector of the Euler angles, and C is the transformation matrix relating body fixed reference frame to orbit fixed reference frame.

In OpSim, a so-called 312-rotation scheme is implemented. In this case, the transformation matrix C is written as:

(3) $$C = \begin{bmatrix} c_2c_3 - s_1s_2s_3 & c_2s_3 - s_1s_2c_3 & -c_1s_2 \\ -c_1s_3 & c_1c_3 & s_1 \\ s_2c_3 - s_1c_2s_3 & s_2s_3 - s_1c_2c_3 & c_1c_2 \end{bmatrix}$$

where $c_i \equiv \cos\theta_i$, and $s_i \equiv \sin\theta_i$ with θ_i being the Euler angle with respect to axis *i*.

4 CONTROL TORQUE

The attitude of the Delfi-C[3] spacecraft is largely determined by the various torques acting on it. The most important parameter is the control torque.

Delfi-C[3] makes use of passive attitude control. Two types of magnetic material are flown. It is common practice to depict the performance of magnetic material in a so-called BH curve, which relates the flux density in the material to the magnetic field strength.

In the longitudinal direction of the spacecraft, i.e. along the *z*-dimension, a permanent magnet is placed. In both lateral directions, i.e. along the *x*- and *y*-dimensions, rods of magnetic hysteresis material are placed. This configuration is shown in figure 2.

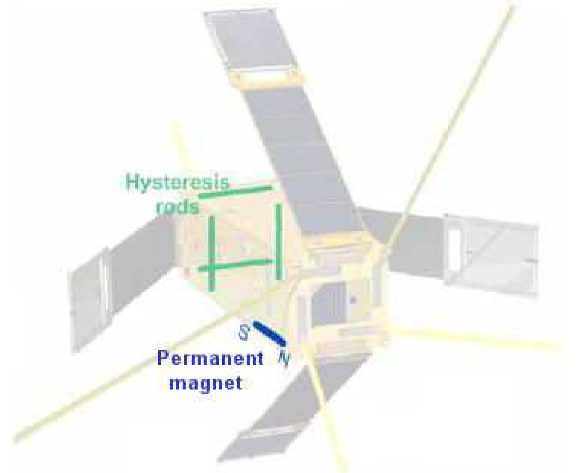

FIG 2: Geometrical configuration of magnetic material

For the permanent magnet, AlNiCo 5 cast magnetic material is chosen. In figure 3, the BH curve corresponding to this material is shown.

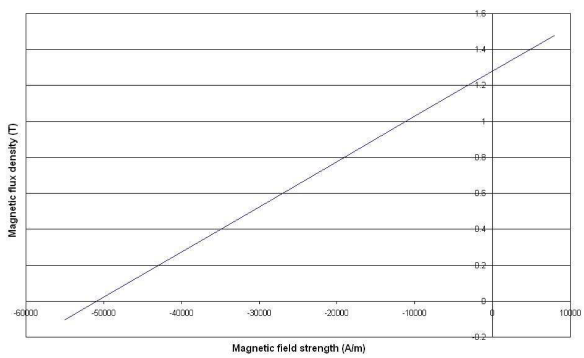

FIG 3: BH curve of AlNiCo 5 cast magnetic material

PermeNorm 5000H2 hysteresis material is applied for the hysteresis rods. This material will dissipate energy when placed in a rotating magnetic field. This is caused because magnetizing the material requires more energy than is released by demagnetizing. In figure 4, the simplified BH curve for PermeNorm 5000H2 hysteresis material is shown.

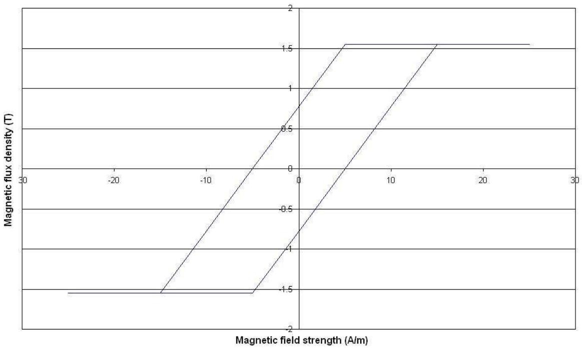

FIG 4: Simplified BH curve of PermeNorm 5000H2 hysteresis material

Behaviour of these materials has been investigated using a Helmholtz cage, which is custom constructed in the clean room at the Faculty of Aerospace Engineering of Delft University of Technology [8].

For evaluating the torque created by the magnetic material, the magnetic field strength caused by Earth magnetic field is calculated [9]. This parameter is governed by:

$$\vec{H} = \frac{\vec{B}_{ext}}{\mu_0} \quad \textbf{(4)}$$

where $\vec{B}_{ext}$ is the magnetic flux density of the Earth magnetic field, and μ_0 is the magnetic permeability in vacuum.

For evaluating the magnetic flux density of the Earth, several models are available. In the OpSim simulator, a simple magnetic dipole model is used [10][11].

With the magnetic field strength known, the magnetic flux density is determined running through the magnetic material using the corresponding BH curves. Then, the so-called magnetization of the material is calculated using:

$$\vec{M} = \frac{\vec{B}}{\mu_0} - \vec{H} \quad \textbf{(5)}$$

The magnetic dipole created by a piece of magnetic material is expressed by:

$$\vec{m} = \vec{M}V \quad \textbf{(6)}$$

where V is the volume of the magnetic material.

As the magnetic dipole represented by the piece of magnetic material has the tendency to align itself with the external magnetic field, a torque will be generated. This torque is expressed by:

$$\vec{T} = \vec{m} \times \vec{B}_{ext} \quad \textbf{(7)}$$

After substituting design values for the volume of the magnetic material, all necessary calculations for determining the control torque can be performed. This yields a magnitude of 10^{-5} Nm for the control torque of the Delfi-C^3 spacecraft.

5 DISTURBANCE TORQUES

In addition, the attitude behaviour of Delfi-C^3 is determined by various disturbance torques acting on the spacecraft along its orbital path. These include the following [12]:

- Gravity gradient torque;
- Aerodynamic torque;
- Solar radiation torque;
- Magnetic disturbance torque.

In the following sections, the magnitudes of the disturbance torques are calculated.

5.1 Gravity gradient torque

Because the moments of inertia about the spacecraft principal axes are not equal, a gravity gradient torque will exist. Deriving an expression for the gravity gradient torque leads to the following result:

$$\vec{M}_{gg} = 3n^2 \cdot \vec{a}_3 \times \hat{J} \cdot \vec{a}_3 \quad \textbf{(8)}$$

where n is the rotational rate of the spacecraft, and $\vec{a}_3 \equiv \vec{R}_c / R_c$, with $\vec{R}_c$ being the position vector of the spacecraft in an Earth fixed reference frame.

As this expression shows the gravity gradient torque in an Earth fixed reference frame, a transformation has to be applied for obtaining the torque in the body fixed reference frame. This transformation yields the following expression:

$$\begin{pmatrix} M_x \\ M_y \\ M_z \end{pmatrix}_{gg} = -\frac{3}{2}n^2 \begin{pmatrix} (J_{yy} - J_{zz})\sin 2\varphi \cos\theta \\ (J_{xx} - J_{zz})\cos^2\varphi \sin 2\theta \\ (J_{yy} - J_{xx})\sin 2\varphi \sin\theta \end{pmatrix} \quad \textbf{(9)}$$

where φ is the Euler roll angle, and θ is the Euler pitch angle.

5.2 Aerodynamic torque

Aerodynamic torque is created by collision of the spacecraft surface with the resident atmospheric particles in the spacecraft's orbit. In general, an aerodynamic drag force is expressed by:

$$\vec{F}_A = \tfrac{1}{2} C_D \rho V^2 A \cdot (\vec{V} \cdot \vec{n}) \cdot \vec{n} \quad \textbf{(10)}$$

where C_D is the drag coefficient of the spacecraft surface, ρ is the mass density of the surrounding atmosphere, $\vec{V}$ is the relative velocity vector of the atmosphere with respect to the spacecraft, $\vec{n}$ is the outward normal vector of the exposed surface, and A is the exposed surface area.

As the aerodynamic drag vector is not likely to go through the center of mass of the spacecraft, a torque will be generated. For a specific surface, the corresponding torque is given as:

$$\vec{T}_A = \vec{F}_A \times (\vec{x}_{CoM} - \vec{x}_{CoP_A}) \quad \textbf{(11)}$$

where $\vec{x}_{CoM}$ is the position of the center of mass of the complete spacecraft, and $\vec{x}_{CoP_A}$ is the position of the center of aerodynamic pressure of the exposed surface.

Adding the contributions of all surfaces leads to the resultant aerodynamic torque acting on the spacecraft.

As the aerodynamic torque depends on the size of the exposed surface area, a dedicated algorithm is developed for taking into account shadowing phenomena. After all, in deployed configuration the solar panels will shadow part of the main spacecraft body. This leads to alteration of the exposed surface area and of the position of the center of pressure.

5.3 Solar radiation torque

Solar radiation torque is generated due to momentum transfer of photons in incident sunlight to the spacecraft. The pressure exerted by the incident photons in case of complete absorption is equal to:

$$p = \frac{S}{c} \quad \textbf{(12)}$$

where S is the solar flux, and c is the speed of light.

Because the spacecraft surface possesses an absorption factor smaller than unity, the expression for the solar radiation pressure force has to take into account the optical properties of the spacecraft.

Assuming no transmission of the incident photons by the spacecraft structure results in the following generated force:

$$\vec{F}_S = (1+R)\frac{\vec{S}\cdot\vec{n}}{c}A\cdot\vec{n} \quad \textbf{(13)}$$

where $\vec{S}$ is the solar flux vector in the body fixed reference frame, $\vec{n}$ is the outward normal vector of the exposed surface, R is the reflectivity factor of the spacecraft surface, c is the speed of light, and A is the area of the exposed surface.

In a similar fashion as for the aerodynamic torque, a solar radiation torque will be produced in case the solar radiation pressure vector is not going through the spacecraft's center of mass. Therefore, the corresponding torque can be expressed by:

$$\vec{T}_S = \vec{F}_S \times \left(\vec{x}_{CoM} - \vec{x}_{CoP_S}\right) \quad \textbf{(14)}$$

where $\vec{x}_{CoM}$ is the position of the center of mass of the complete spacecraft, and $\vec{x}_{CoP_S}$ is the position of the center of solar radiation pressure of the exposed surface.

By adding all contributions generated by the individual surfaces, the solar radiation torque acting on the spacecraft is obtained.

Similarly as for the aerodynamic torque, shadowing effects of the solar panels are taken into account in assessing the magnitude of the solar radiation torque.

5.4 Magnetic disturbance torque

Magnetic disturbance torques are produced due to interaction of electrical currents with the Earth magnetic field.

One of the forces involved in the generation of magnetic disturbance torques is the Lorentz force, which is generated if an electrical current is flowing in a magnetic field. It is expressed by:

$$\vec{F}_m = \sum\left(\vec{B}\times I\,\vec{l}\right)_i \quad \textbf{(15)}$$

where $\vec{B}$ is the external magnetic field, I is the electrical current flowing through current carrying wire i, and $\vec{l}$ is the length of current carrying wire i.

As the resultant vector will not likely go through the center of mass of the spacecraft, a torque is produced.

Another source of disturbance torque is caused by magnetic induction. As the rotational rate of the spacecraft will lead to a change in magnetic flux, voltages are induced in electrical conducting material. These voltages lead to current flows, which consequently result in a generation of torque.

6 POWER EVALUATION

To determine the maximum useful electrical load of the Delfi-C^3 spacecraft, the minimum amount of array power in orbit is calculated. For this purpose a custom algorithm has been developed.

Solar flux at the orbital position of the Delfi-C^3 spacecraft is determined by evaluating the position of the sun with respect to the Earth. As the orbital position of Delfi-C^3 is known, the sunlight vector can be written as:

$$\vec{r}_{S/D} = \vec{r}_{S/E} + \vec{r}_{E/D} \quad \textbf{(16)}$$

where $\vec{r}_{S/E}$ is the positional vector of the Earth in the heliocentric reference frame, and $\vec{r}_{E/D}$ is the position of Delfi-C^3 in the geocentric reference frame.

In addition to solar flux, albedo flux is taken into account by dividing the hemisphere of the Earth directed to the spacecraft into 180 parts. For every part, the corresponding albedo flux is determined. The complete albedo flux is obtained by summing all individual contributions.

The incident flux is evaluated by introducing the normal vector of the involved solar array. This parameter is governed by:

$$Q = S\cdot\vec{r}_s\cdot\vec{n} + a_j S\cdot\left(\vec{r}_a\right)_j\cdot\vec{n} \quad \textbf{(17)}$$

where S is the solar flux, $\vec{n}$ is the outward normal vector of the involved solar panel, $\vec{r}_s$ is the unit direction vector from the solar panel to the Sun, a_j is the albedo factor of part j of the Earth globe, and $\left(\vec{r}_a\right)_j$ is the unit direction vector from the solar panel to part j of the Earth globe.

In the process of determining the array power, it is assumed that the solar cells are operating in their maximum power point. The power generated on a solar array is computed by:

$$P = \eta Q \quad \textbf{(18)}$$

where η is the efficiency of the solar cells.

The value of efficiency of the solar cells depends on several factors. An important factor is the cell temperature. In general, the performance of a solar cell decreases with increasing temperature. The influence of temperature on the performance is governed by [12]:

$$\eta' = \eta_{ref} + \lambda\left(T - T_{ref}\right) \quad \textbf{(19)}$$

where η_{ref} is the efficiency of the photovoltaic cells at the reference temperature, λ is the temperature coefficient of the array power, and T_{ref} is the reference temperature.

Another influence on the array power is the mission duration. After all, exposure of the cells to UV radiation will lead to a decrease in their performance. Therefore, the efficiency of the photovoltaic cells is expressed by:

$$\eta = \eta'\cdot(1-\mu)^t \quad \textbf{(20)}$$

where μ is the annual degradation of the photovoltaic cells, and t is the mission duration in years.

The actual power available from the solar arrays depends on the operation of the electrical power system. As the system does not always operate in the maximum power point a correction factor is introduced. This leads to the following expression:

(21) $$P = k\eta Q$$

where k is the power correction factor set to 0.8.

7 SIMULATION RESULTS

Various simulations have been performed to verify the compliance of the spacecraft design to the requirements. Three different test scenarios have been investigated. The scenarios are listed in the table 3.

TAB 3: Characteristics of the simulation scenarios

Scenario	Initial rotational rate	Panel deployment angles
Nominal	0 rad/s	4 × 35°
Fast rotating	0.175 rad/s about x-axis	4 × 35°
Single solar panel deployment failure	0 rad/s	3 × 35°, 1 × 0°

For all scenarios, both the stowed and deployed configurations have been investigated.

7.1 Spacecraft requirements

The following requirements are of relevance for the simulations:

- Minimum available array power in sunlit conditions and all panels deployed shall exceed 3 W;
- Components of the satellite rotational rate shall be kept below 0.175 rad/s (10 deg/s) for all body axes;
- Average absolute spacecraft rotational rate with respect to sun vector shall be in excess of 0.0087 rad/s (0.5 deg/s);
- Field of view of autonomous wireless sun sensor (AWSS) shall contain Sun for a significant part of the orbit;
- In sunlit conditions and stowed configuration, array power shall equal at minimum 2.5 W in periods of at least 30 s.

7.2 Simulation conditions

The following conditions hold for every performed simulation.

With respect to the temperature of the solar cells, no real-time thermal model has been implemented in OpSim. Instead, the temperature of the cells is taken constant at the worst case temperature of 50 °C. This temperature has been determined using a thermal model of the spacecraft [13].

The spacecraft is in stowed configuration during launch and during initial operations. At 1800 seconds after separation, the appendages are deployed. In the simulations, the deployment procedure is assumed to occur instantaneously. In reality, the panels are deployed sequentially, each taking less than 1 minute to deploy.

Table 4 summarizes the Delfi-C^3 geometrical characteristics and mass properties used in the simulations.

TAB 4: Relevant geometrical characteristics of the Delfi-C^3 spacecraft

Parameter	Value
Moment of inertia x-axis	$3.494\cdot10^{-2}$ kg·m^{-2}
Moment of inertia y-axis	$3.494\cdot10^{-2}$ kg·m^{-2}
Moment of inertia z-axis	$1.505\cdot10^{-2}$ kg·m^{-2}
z-position of center of mass w.r.t. geometrical center	-1.1 mm

The electrical characteristics of the applied photovoltaic cells required for simulating the available array power are listed in table 5 [5].

TAB 5: Relevant electrical characteristics of the Delfi-C^3 spacecraft

Parameter	Value
Open circuit voltage @ 28 °C	2.47 V
Short circuit current @ 28 °C	0.389 A
Max power point voltage @ 28 °C	2.13 V
Max power point current @ 28 °C	0.366 A
Open circuit voltage temperature coefficient	-5.5 mV·K^{-1}
Short circuit current temperature coefficient	0.146 mA·K^{-1}
Max power point voltage temperature coefficient	-5.1 mV·K^{-1}
Max power point current temperature coefficient	0.141 mA·K^{-1}
Number of cells in single string	5
Number of strings in single array	1

7.3 Array power

In this section, the available array power of the Delfi-C^3 spacecraft is examined for the three simulation scenarios.

In figure 5, the power profiles of Delfi-C^3 for the different scenarios in stowed configuration including deployment activities are shown.

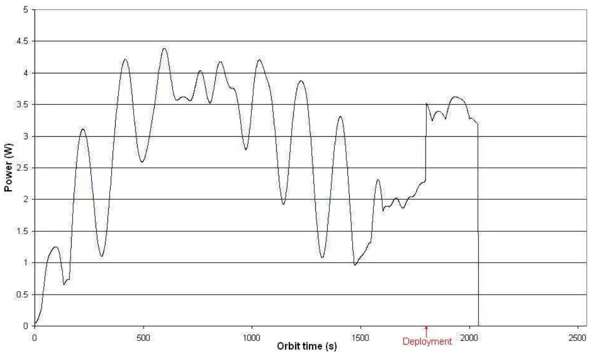

a.

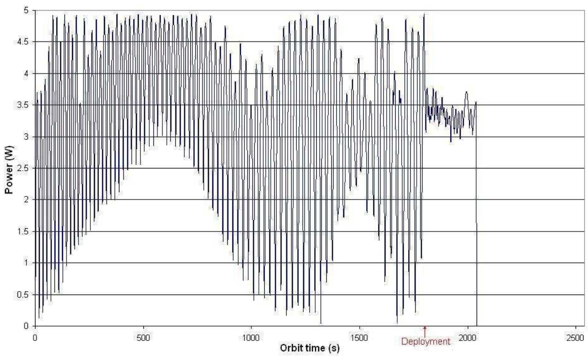

b.

FIG 5: Available array power profile including panel deployment a. nominal scenario; b. fast rotating scenario

In the nominal scenario, the array power shows a large variation in magnitude before the deployment of the appendages. This is due to blind spots, in which no solar flux is captured by the arrays. On the other hand, the maximum available power is very large reaching values of 4.5 W.

The array power shows a large variation in the fast rotating scenario as well. Due to the high initial rotational rate, a fast oscillation is present. This leads to a variation of the array power between 0 W and 5 W.

This fast oscillation could lead to problems in powering the spacecraft deployment systems. However, a slow oscillation is noticed in the magnitude of minimum power. Hence, during part of the orbit sufficient power (>2.5 W) is present for deploying the appendages.

In the panel deployment failure scenario, no changes are found with respect to the nominal situation until deployment. This comes as no surprise, because in stowed configuration the spacecraft is geometrically exactly the same.

The Delfi-C^3 power profiles for the deployed configuration are shown in figure 6.

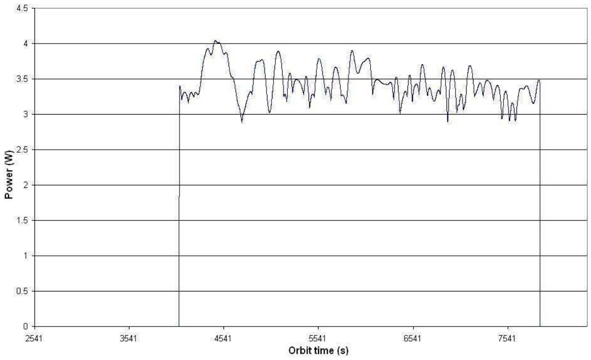

a.

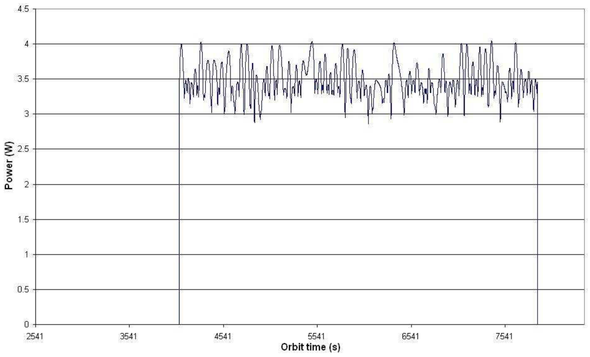

b.

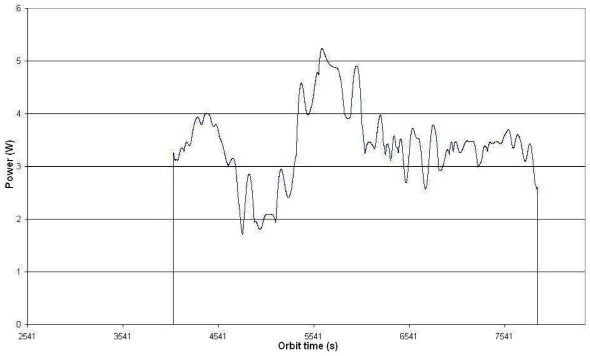

c.

FIG 6: Available array power in deployed configuration a. nominal scenario; b. fast rotating scenario; c. panel deployment failure scenario

Compared to the stowed configuration, the variation in array power is significantly decreased. A maximum value of 4W in available power is noticed, while the minimum power drops slightly below 3 W.

In the fast rotating scenario, the fast oscillation noticed in stowed conditions is still present in deployed configuration. The minimum power value increases to slightly below 3W. Furthermore, the maximum power value decreases to approximately 4 W.

In the panel deployment failure scenario, the minimum and maximum power show significant changes compared to the stowed configuration. The maximum power shows a slight increase to 5.2 W, which is explained by the existence of an attitude with good incidence angles for multiple solar panels.

The decrease in minimum power is more serious. As the worst case situation yields bad incidence angles for the solar panels, the minimum power reaches only 1.7 W. These periods can occur for a reasonably long time limiting the spacecraft operation.

In case of a single deployment failure, the requirements are not met. The minimum available power is smaller than the required power, which will lead to temporary black-outs of the spacecraft. Although is not a complete failure of the spacecraft's mission, the useful mission time is reduced.

In the nominal and fast rotating scenario, the design requirements are met.

7.4 Rotational velocity

In this section, the rotational velocity of the Delfi-C^3 spacecraft in the three scenarios is investigated.

In figure 7, the rotational velocity of Delfi-C^3 during the initial three orbits is shown.

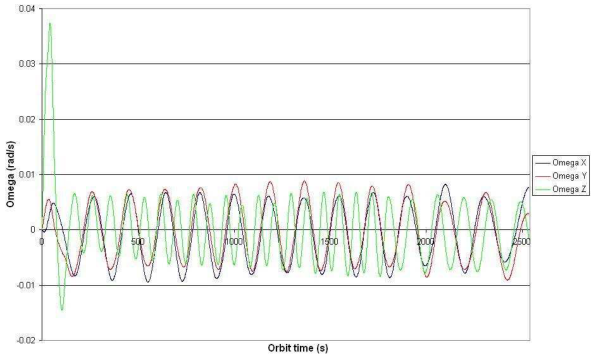

a.

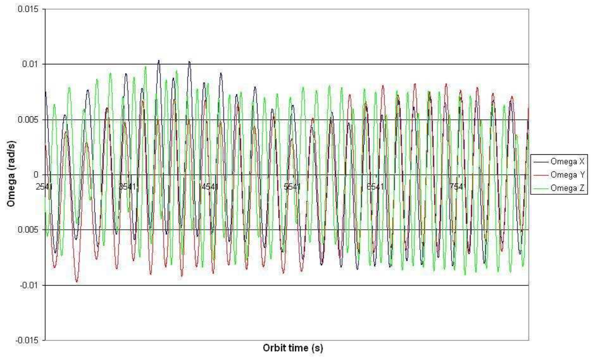

b.

FIG 7: Rotational velocity during Delfi-C^3 initial operations in nominal scenario a. orbit 1; b. orbit 2

The figure shows that although no initial rotational velocity is present, the spacecraft spins up. Cross-coupling leads to the appearance of oscillations in the rotational velocity about the body axes. By analyzing this plot, this spin-up reaches a rotational speed of 0.0087 rad/s (0.5 deg/s) in steady-state.

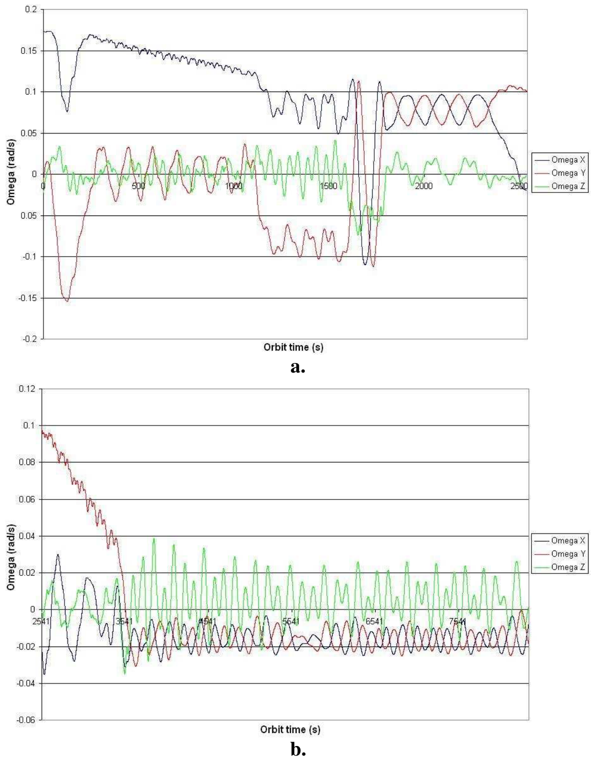

FIG 8: Rotational velocity during Delfi-C[3] initial operations in fast rotating scenario

a. orbit 1; b. orbit 2

Figure 8 shows that the rotational velocity starts out at 0.175 rad/s (10 deg/s). A rapid decrease is noticed, which is the result of the hysteresis rods. It is derived that the rotational speed reaches a steady state value of 0.026 rad/s (1.5 deg/s) after 4000 s. This settling time is slightly longer than a single orbital period. Hence, the hysteresis rods are extremely successful at damping the rotational rate of the spacecraft.

In the panel deployment failure scenario, no significant differences in the rotational velocity could be distinguished with respect to the nominal scenario. This is explained by the dominating torque produced by the magnetic material, which is significantly larger than the disturbance torques.

In all three scenarios, the design requirements are met. The rotational velocity remains below the upper boundary of 0.175 rad/s and above the lower boundary of 0.0087 rad/s.

7.5 Spacecraft attitude

In the following plots, the spacecraft attitude in the period between 2000 s and 3800 s is shown. This period illustrates a representative orbit of the Delfi-C[3] spacecraft.

In figure 9, the projection of the positive z-axis in the body reference frame on the celestial sphere is shown. Two different plots are shown, which correspond with the two hemispheres. One shows the projection on the hemisphere encompassing the Earth, while the other gives the projection on the hemisphere pointing away from the Earth.

In these plots, the positive x-axis corresponds with the velocity vector of the spacecraft. Furthermore, the y-axis denotes the cross track direction. The origin of the first plot is the vector to the center of Earth (i.e. nadir), while the origin of the other plot corresponds with the vector away from the center of Earth (i.e. zenith).

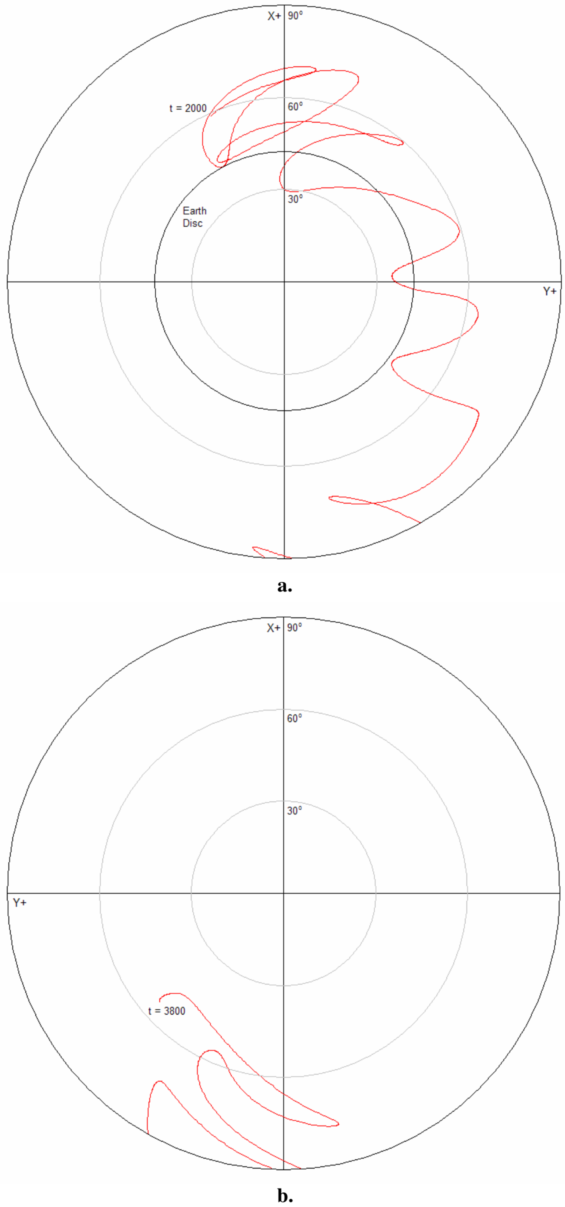

FIG 9: Projection of the positive z-axis on the celestial sphere

Figure 9 shows that at the beginning of the time period (t = 2000 s), the spacecraft is pointing in the direction of flight. With respect to nadir, it is at an angle of approximately 60°.

It continues to oscillate about a fixed point. However, after some time the spacecraft attitude changes. The positive z-axis has the tendency to make a 180° turn. This is done in an oscillatory motion.

At the end of the period (t = 3800 s), the spacecraft is pointing with its back towards the direction of motion. The positive z-axis is at an angle of approximately 60° with respect to zenith.

An explanation for the shift in attitude is found in the change of the Earth magnetic field. As the magnetic material in the spacecraft is aligning the spacecraft with the Earth magnetic field, a pass of the spacecraft over the magnetic poles leads to a 180° turn.

In figure 10, the position of the Sun in relation to the spacecraft body is shown. Hence, the axes in the figures correspond to the body fixed reference frame.

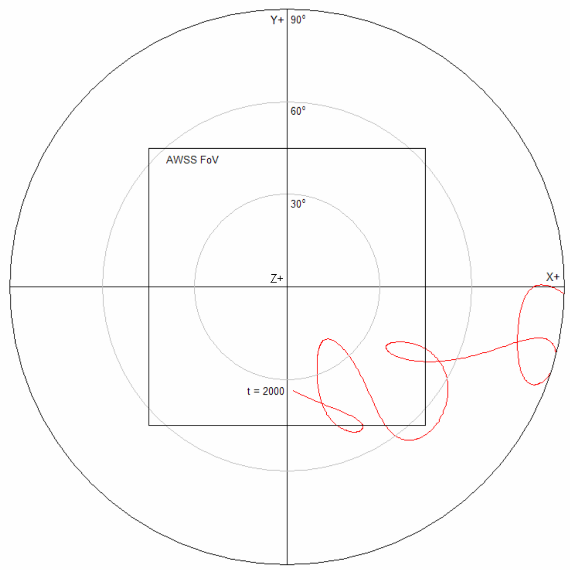

a.

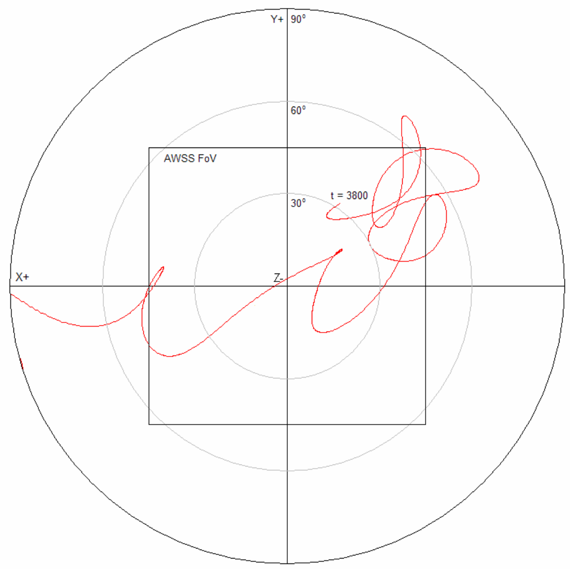

b.

FIG 10: Projection of the Sun position on the celestial sphere

In this figure the fields of view of both autonomous wireless sun sensors (AWSS) are shown. These sensors are positioned in the square front and back panels.

At the beginning of the time period, the Sun is positioned in front of the spacecraft. However, it dwindles via the side of the spacecraft to the back. At the end, the position oscillates slightly, which seems to indicate that the spacecraft remains in a more-or-less fixed attitude with respect to the Sun. Recalling Delfi-C^3's orbit, this resembles a pass over a geographic pole.

It can be concluded that the requirement with respect to the field of view of the AWSS is fulfilled. For a large part of the orbit, the Sun is observed by the AWSS. In the shown period, the position of the Sun even travels through all four quadrants of the back AWSS field of view.

In figure 11, the projection of the magnetic field vector in the body fixed reference frame is shown. This projection is plotted in similar fashion as in figure 10, by using a sphere encompassing the spacecraft with infinite radius.

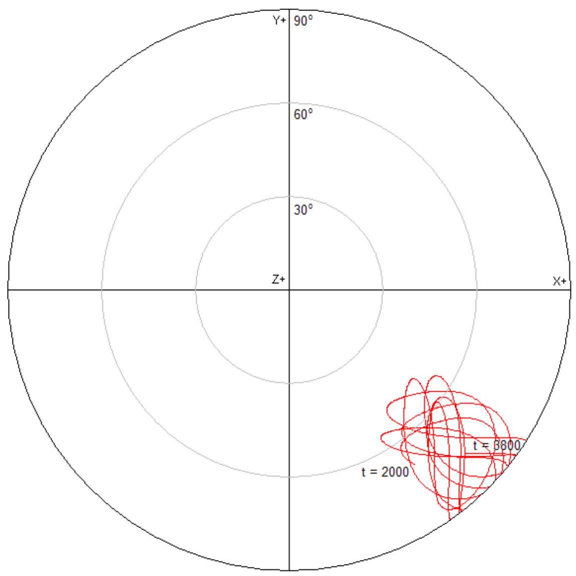

a.

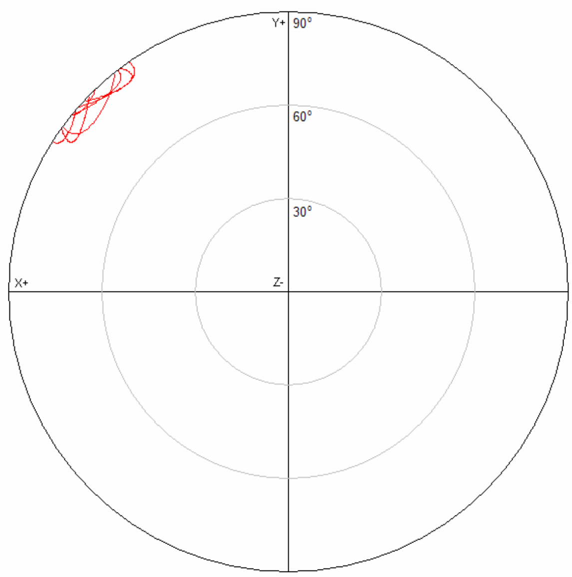

b.

FIG 11: Projection of the magnetic field vector on the celestial sphere

The figure shows that the magnetic field projection oscillates about a fixed point. Throughout the entire time period, no large deviations with respect to this point are present. Therefore, it can be concluded that the spacecraft is in magnetic lock, which means that the magnetic torque is sufficiently large to make the spacecraft follow any change in the direction of the magnetic field. This conception is reinforced by the magnetic torque being a factor 100 larger in magnitude than the largest disturbance torque (10^{-5} Nm versus 10^{-7} Nm).

The exact position of the epicenter of the oscillation coincides with the resultant dipole vector of the magnetic material in Delfi-C^3. This position is at an off-set angle of 70° with respect to the spacecraft's *z*-axis with an amplitude of approximately 30°.

7.6 Simulator limitations

A remark has to be placed at the application of the OpSim simulator for Delfi-C^3. It has been found that the simulation algorithms are extremely sensitive to the choice of time step. Choosing too large time steps leads to numerically instable results.

This restriction results in a maximum simulation duration of several days. The complete mission duration of Delfi-C^3 could not be simulated. It is expected that the overall minimum values will not deviate from the corresponding values found in the simulations of the initial orbits.

8 CONCLUSIONS

For simulation of the performance of the Delfi-C^3 spacecraft, use is made of the OpSim operational simulator. Successful simulation was accomplished by introduction of specific algorithms for control and disturbance torques, and available array power.

Three different scenarios were simulated and the results were evaluated using the design requirements for available array power and rotational velocity.

In stowed configuration, the array power shows large variations. Conditions yielding zero power are possible, which will lead to a reboot of the spacecraft.

In deployed configuration, the minimum required power of 3W is always generated. Rotational rate has no influence on this. In case a single solar panel fails to deploy, large dips in array power are experienced. During these situations, the solar arrays are not capable of supplying the complete spacecraft with electrical power.

When the spacecraft possesses no initial rotational velocity, a spin-up is accomplished to approximately 0.5 °/s. No influence is found by introducing asymmetry by failing to deploy a solar panel.

A high initial rotational velocity results in a decrease in rotational rate due to the hysteresis rods. Steady state rotation equals approximately 1.5 °/s.

Investigation of the attitude profile shows that the spacecraft is in a coarse magnetic lock. Its positive *z*-axis does not deviate from the magnetic field vector by more than 30°.

REFERENCES

[1] L. Meijer, *Power model design for the Smart-1 Project Test Bed*. Delft University of Technology, The Netherlands, 2001.

[2] B. Naber, *Power model design and Image Generation System implementation of the Delfi-1 Simulator*. Delft University of Technology, The Netherlands, 2005.

[3] R. Raus, *Design of the ADCS of Delfi-1 using the satellite simulator OPSIM*. Delft University of Technology, The Netherlands, 2006.

[4] A.A. Vaartjes, W.J. Ubbels, and R.J. Hamann, *The Delfi-C^3 Nanosatellite*. Proceedings of 1st Hellenic-European Student Space Science and Technology Symposium, Patras, Greece, 2006.

[5] J.H. Doorn, *Delfi-C^3's Electrical Power System and its Thin Film Solar Cell Payload*. Delft University of Technology, The Netherlands, 2006.

[6] E.D. van Breukelen, *Delfi-C^3 Satellite: Design of the Command and Data Handling System and Attitude Control System*. Delft University of Technology, The Netherlands, 2006.

[7] Bong Wie, *Space Vehicle Dynamics and Control*. AIAA Education Series, 1998.

[8] F.M. Poppenk, R. Amini, and G.F. Brouwer, *Design and Application of a Helmholtz Cage for Testing Nano-Satellites*. Delft University of Technology, The Netherlands, 2007.

[9] J.F. Levesque, *Passive Magnetic Attitude Stabilization using Hysteresis Materials*. Université de Sherbrooke, Quebec, Canada, 2004.

[10] R.F. Butler, *Paleomagnetism: Magnetic Domains to Geologic Terranes.* Blackwell Scientific Publications, Oxford, United Kingdom, 1992.

[11] T.F. Tascione, *Introduction to the Space Environment*. Second Edition. Krieger Publishing Company, Malabar, Florida, United States of America, 1994.

[12] J.R. Wertz, and W.J. Larson (editors), *Space Mission Analysis and Design*. Third edition. Microcosm Press, El Segundo, California, United States of America, 1999.

[13] J. Rotteveel, *Flexible Systems Engineering and Thermal Control Tools for Delfi-C^3*. Delft University of Technology, The Netherlands, 2006.